Self-Learning Network-based segmentation for real-time brain M.R. images through HARIS

Naga Srinivasu Parvathaneni [Equal first author, 1], **Valentina E. Balas** [Corresp. Equal first author, 2]

[1] Department of Computer Science and Engineering, GITAM Institute of Technology, GITAM Deemed to be University, Visakhapatnam, Andhra Pradesh, India

[2] Department of Automation and Applied Informatics, Aurel Vlaicu University of Arad, Arad, Romania

Corresponding Author: Valentina E. Balas
Email address: balas@drbalas.ro

In recent years in medical imaging technology, the advancement for medical diagnosis, the initial assessment of the ailment, and the abnormality have become challenging for radiologists. Magnetic Resonance Imaging is one such predominant technology used extensively for the initial evaluation of ailments. The primary goal is to mechanizean approach that can accurately assess the damaged region of the human brain throughan automated segmentation process that requires minimal training and can learn by itself from the previous experimental outcomes. It is computationally more efficient than other supervised learning strategies such as CNN deep learning models. As a result, the process of investigation and statistical analysis of the abnormality would be made much more comfortable and convenient. The proposed approach's performance seems to be much pleasing compared to its counterparts, with an accuracy of 77% with minimal training of the model. Furthermore, the performance of the proposed training model is being evaluated through various performance evaluation metrics like sensitivity, specificity, Jaccard Similarity Index, and Mathews correlation coefficient, where the proposed model is productive with minimal training.

Self-Learning Network-based segmentation for real-time brain MR images through HARIS

7   P Naga Srinivasu[1], Valentina E. Balas[2]

9   [1] Department of Computer Science and Engineering, GIT, GITAM Deemed to be University,
10 Visakhapatnam-530045, AP, India
11 [2] Department of Automation and Applied Informatics, Aurel Vlaicu University of Arad,
12 Romania

14 Corresponding Author:
15 Valentina E. Balas[2]
16 Aurel Vlaicu University of Arad, Romania
17 Email address: balas@drbalas.ro

Abstract

In recent years in medical imaging technology, the advancement for medical diagnosis, the initial assessment of the ailment, and the abnormality have become challenging for radiologists. Magnetic Resonance Imaging is one such predominant technology used extensively for the initial evaluation of ailments. The primary goal is to mechanize an approach that can accurately assess the damaged region of the human brain through an automated segmentation process that requires minimal training and can learn by itself from the previous experimental outcomes. It is computationally more efficient than other supervised learning strategies such as CNN deep learning models. As a result, the process of investigation and statistical analysis of the abnormality would be made much more comfortable and convenient. The proposed approach's performance seems to be much pleasing compared to its counterparts, with an accuracy of 77% with minimal training of the model. Furthermore, the performance of the proposed training model is being evaluated through various performance evaluation metrics like sensitivity, specificity, Jaccard Similarity Index, and Mathews correlation coefficient, where the proposed model is productive with minimal training.

Keywords: MR images; Segmentation; CNN; HARIS; Self-Learning Network;

Introduction

Medical imaging technology has been critical in medical diagnostics for accurately detecting the presence of malignant tissues in the human body. There are divergent imaging technologies that are available for diagnosis of abnormality among various organisms that includes

41 X-Ray technology, as stated by (Vaga & Bryant, 2016), Computed tomography (CT) technology,
42 as stated by (Venkatesan et al., 2017), Magnetic Resonance Imaging (MRI) technology (Chahal et
43 al.,2020),(Srinivasu et al., 2020) and positron emission tomography (PET) scan (Norbert et al.,
44 2017), (Schillaci et al., 2019). All the approaches mentioned above are non-invasive and capable
45 of diagnosing malignant tissue efficiently. In many cases, imaging technology is aptly suitable for
46 identifying abnormalities in the human body. It would help the physician provide better treatment
47 and assist in planning the clinical procedure. The current study has focused on mechanizing a
48 model capable of diagnosing the MR imaging and estimating the extent of the damage.
49   Medical imaging technology has upgraded stupendously to elaborate every minute and tiny
50 ailment in the human body that could efficiently diagnosed disease at a significantly earlier stage.
51 The proposed study primarily focused on tumor identification and volumetric estimation of the
52 tumorous region in the human brain. There are numerous machine learning models available for
53 accurately identifying the tumorous regions from MR images. Yet, most of these techniques are
54 imprecise, process thirsty, and particularly semi-automated procedures used in tumor
55 identification. To circumvent the limitations of the above methodologies, several automated
56 techniques, including the conventional models like Genetic Algorithm (GA), as stated by
57 (Srinivasu et al.,2020), Artificial Neural Networks (ANN), as said by (Wentao et al., 2020) and
58 Deep Learning techniques as mentioned by (Deepalakshmi et al., 2020), (Srinivasu et al., 2021).
59   As part of recognizing ailments, several stages, including pre-processing the MR images
60 to address noise in the original MR images, such as Spackle noise, Poisson noise, and Gaussian
61 noise, are introduced into the image at various stages during the process of rendering the image.
62 And the pre-processed step will enhance the contrast and the texture of the image that assist in a
63 faster and convenient way to recognize the malignant tissues. Once the noise in the image is pre-
64 processed, the MR image is fed to remove the skull region. Then the MR image is segmented to
65 recognize the malignant region, followed by the volumetric estimation for analyzing the impact of
66 the damage. The results of the automated segmentation approaches are refined over multiple
67 iterations for the precise outcome.
68   Generally, the medical images are segmented to locate the abnormal regions in the image
69 based on texture-based information. The process of image segmentation plays a vital role in the
70 identification of the malignant areas in the MR image; There are various semi-automated and
71 automated ways of segmenting the MR images that could efficiently segment the images, but there
72 is a considerable tradeoff between the accuracy and the computation efforts put forward by each
73 of those approaches. Supervisory models yield better accuracy, but they need tremendous training
74 data that needs more computational resources.
75   K-Mean's algorithm is one such semi-automated approach that segments the MR Image
76 based on the pre-determined number of segments as stated by (Alam et al., 2019), (Chahal et al.,
77 2020). Thus, the proposed approach is one of the simple techniques for the segmentation of the
78 images. But the major drawback of this approach is that the total number of segments is fixed well
79 before the segmentation has begun. Therefore, if the k value is too large, it would lead to over-
80 segmentation, and if the k value is too small, it will lead to under-segmentation of the image.

81   Segmentation of MR images is indeed possible using completely automated techniques
82   such as thresholding, as stated by (Sowjanya et al., 2018), (Kumar et al., 2015). The threshold-
83   based method works comparatively better in the homogeneous image, but accuracy mainly
84   depends on the approximated threshold value. A minimal deviation from the ideal value of the
85   threshold results in an exponential variance in the segmented image.
86   The other predominantly used segmentation technique through Region Growing (Dalvand
87   et al., 2020) strategy that can effectively handle the problem of over and under segmentation often
88   encountered in K-Means-based approaches. The experimental studies on the Region Growing-
89   based approach are proven to improve the sensitivity and specificity for precise identification of
90   the malignant region in the human brain (Punitha et al., 2018). But the seed point must be chosen
91   appropriately, which needs tremendous efforts in recognizing the optimal seed point. If the initial
92   seed points are inappropriately chosen, the entire process of segmentation of the image goes
93   wrong, and also this approach needs computationally more effort.
94   (Sheela et al., 2020), (Mathur et al., 2016) proposed Edge Based Segmentation for image
95   segmentation, a relatively simplistic approach. But in the suggested edge-based approach, the
96   image must be pre-processed rigorously to elaborate the edge-related information, which involves
97   high computational efforts. (Pandav, 2014), (Liang&Fu, 2018), (Kornilo et al., 2018) has proposed
98   Watershed-based image segmentation that effectively addresses limiting the number of segmented
99   areas identified using edge information by marker-controlled watershed-based segmentation. The
100 process of limiting the segments will assist in avoiding the over-fitting problem that is experienced
101 in the majority of the user intervened models and the supervised models. But in watershed-based
102 segmentation, considerable efforts are needed during pre-processing phase to separate the
103 foreground and background regions in the image. (Sudharania et al., 2016) have proposed
104 Morphological based segmentation that exhibits an exceedingly high accuracy in less intensity MR
105 images. But it needs several iterations to converge to a better solution, which needs more
106 computational efforts.
107   (Jude et al., 2015),(Madallah et al., 2020),(Verma et al., 2015) has proposed Fuzzy C
108 Means(FCM)based MR image segmentation is a highly accurate, well-founded, and rapid
109 approach that effectively handles the uncertain situation of allocating pixels among multiple
110 segments through distributing pixels to the appropriate segment depending on the membership
111 value determined at each iteration. In fuzzy-based segmentation, the pixels are assigned to their
112 corresponding region based on the membership function value that lies in a range of 0 to 1. The
113 value 1 indicates the corresponding pixel is more likely to be associated with the corresponding
114 segment. The biggest problem with the FCM technique is determining the membership value at
115 each iteration for all pixels in the image that need additional processing efforts. In addition, the
116 adjustment of the bottom and upper approximated for the randomness is complex though FCM.
117   (Al-Shamasneh et al., 2020) have suggested an MR image segmentation through Contour
118 Based segmentation that efficiently recognizes various brain tissues for both homogeneous and
119 heterogeneous malignant cases. But it is not much efficient for noisy images and high-intensity
120 images. (Li et al., 2018) have proposed a Level Set centric technique for the MR image

121   segmentation based on the pre-approximated threshold value. The level set method is a very
122   complex approach, and the approximated threshold value determines the efficiency of the
123   approach's segmentation.

124   (Wang et al., 2019), (Diaz & Boulanger, 2015) have proposed Atlas Based Segmentation
125   for MR images is a straightforward approach that employs segmentation of the MR images. It is
126   computationally faster than used labeling, and it is independent of the deformation model. The
127   suggested approach merges the intensity template image and segmented reference image to register
128   to further segment the image. In the atlas-based approach, choosing the initial seed point is crucial
129   as the entire segmentation scenario is based on the seed point selection. However, the efficiency
130   of this approach is based on the precision of the topological graph.

131   (Venmathi et al., 2019), (Liu et al., 2018) have proposed Markov Random Field (MRF) to
132   segment the MR image through the Gaussian mixture model that supports incorporating the
133   neighboring pixels association in practical and mathematical perception. The method works on
134   textured-based information. Markov random field-based approach for the segmentation of the
135   image includes spatial information that aids in normalizing noise and overlapping the neighboring
136   regions. (Javaria et al., 2019) have suggested an approach that used the spatial vector alongside
137   Gabor decomposition that distinguishes the malignant and non-malignant tissues in the MR image
138   of the Bayesian Classifier. Despite the accuracy, MRF needs more computational efforts and the
139   process of picking the parameters systematically.

140   (Varuna et al.,2018), (Gibran et al., 2020) have suggested Probabilistic Neural Network
141   (PNN) in combination with Learning Vector Quantization (LVQ) that assists in reducing the
142   computational time by optimizing all the hidden layers in the proposed method. The region of
143   interest that must be recognized for designing the network must be done carefully, as image
144   segmentation quality depends on the exactness of the region of interest. (Sandhya et al., 2020),
145   (Mei et al., 2015), (De & Guo, 2015) have suggested a Self-Organized Map (SOM) based
146   algorithm for segmentation of the MR image that includes the spatial data and the grey level
147   intensity information in the segmentation of the image. It is outstanding in separating the malignant
148   tissues. But the SOM engine has to be trained rigorously for better accuracy. The quality of the
149   image segmentation is directly dependent on the training set. Mapping is one of the complicated
150   tasks in a SOM-based approach.

151   (Havaei et al., 2016), (SivaSai et al., 2021), (Wentao et al., 2020) have proposed a Deep
152   Neural Networks-based approach that is computationally efficient and highly precise in
153   determining the abnormality from the medical image. Yet, the primary problem is that the
154   implementation procedure and machine must be computationally efficient with adequate
155   processing resources to perform the image segmentation in a reasonable time, which is not always
156   technically feasible.

157   (Sachdeva et al., 2016) have suggested multiple hybrid approaches for the segmentation of
158   the MR images. The multiclass categorization of malignant tissues is done efficiently, and high
159   accuracy is attained through machine learning and soft computing techniques. Pulse Coded Neural
160   Network (PCNN) is a technique used in coherence with the semi-automated methods for better

161 segmentation. While segmenting the MR image, the Region of interest could be perceived as a
162 region growing approach that selects the initial points assumed as the seed points in the earlier
163 stages. Secondly, a Feed Forward Back Neural Network (FFBNN) selects the seed points that send
164 back the input until the input turns uniform. (Qayyum et al., 2017) have attained multiple sub-
165 images with multi-resolution data by employing Stationary Wavelet Transform (SWT). The spatial
166 kernel is being applied over the resultant sub-images to locate the demographic features. With the
167 help of extracted features and the Stationary Wavelet Transform coefficient, the multi-dimensional
168 features are built. The identified features and coefficients as the input to the self-Organized map,
169 Linear vector Quantization, are finally used to refine the results.

170   (Srinivasu et al., 2020) has proposed an approaches Twin Centric Genetic Algorithm with
171 a Social Group Optimization that has produced a precise outcome in tumor identification from the
172 brain MR images. The twin-centric GA model is comparatively faster than the conventional GA
173 approach, with a faster crossover rate that results in a new segment. The mutation operation is
174 performed based on the fitness value to reform them with other strongly correlated regions in the
175 image. The outcome of the Twin GA is being refined through the Social Group Optimization
176 approach, which has refined the outcome through selecting the appropriate features in the image
177 for the segmentation. (Dey et al., 2018) has experimented with the SGO approach in fine-tuning
178 the outcome of the classification. The current approach is comparatively faster, but in performing
179 the two-point crossover, there is a chance of diverging from the optimal number of regions and
180 may end up with the over-fitting issue. And the execution of two high computational algorithms
181 needs a significant computational effort to segmentation the MR image.

182   The main objective is to formulate a mechanism that can efficiently segment the real-time image
183 into multiple regions based on the available features by minimizing the computation efforts. The proposed
184 approach is a self-trained strategy that upskills the algorithm with some pre-existing real-time scenarios.
185 Previous experimental results show that the proposed SLNS algorithm can differentiate the skull region
186 from the brain tissues in the MR image without any external pre-processing algorithm. It can quickly
187 extricate brain tissues from the non-brain tissues through the available feature set. The proposed model
188 is robust in handling the images with an acceptable noise level, and it needs less computational
189 effort for training the model. The experimentation has been performed to evaluate the accuracy of
190 the proposed approach, and the upshot seems to be promising.

191

192 ## Self-Learning Network Based Real-Time Segmentation

193   Cognitive technology in real-time image segmentation is a multidisciplinary technique that
194 is an intrinsic aspect of Fully Convolutional Neural Networks. Fully Convolutional Neural
195 Networks are widely utilized in real-world settings to successfully handle 2D images. The concept
196 of semantic segmentation has been used in coherence with multi-objective function-based
197 algorithms for better results. The weak learning network is based on the partial training of the
198 algorithm and the tuning of the algorithm so that it would be able to differentiate among multiple
199 classes. In addition, the algorithm is capable of training itself for better efficient segmentation of
200 the image. In every stage of execution for evaluating the tumor's region from the MR image, the

201   proposed method would segment the image based on the trained information. The resultant
202   segmented imaged would be further refined in further network layer's multi-objective functions.

Partial Training of The Algorithm

204   In contrast to its competitors, the suggested methodology is a partly trained strategy that
205   does not need extensive training. As shown by (Xiao et al., 2015), the recommended strategy
206   involves training the original image with an acceptable quantity of noisy data to ensure that the
207   algorithm can address noise images. Additionally, the noise picture is specified in the labels. The
208   binary identifier notion is used to distinguish a noisy picture from a non-noise labeled image (Misra
209   et al., 2016). It has proposed the idea of independently labeling the noise class. The role of
210   differentiating the image-based noise classes is significantly essential. The image could be easily
211   determined among the noise levels to process the images based on the noise variance.
212   The model is being trained to distinguish brain tissues from non-brain tissues such
213   as brain fluids, the skull region, the thalamus, and the brainstem, which must be isolated from brain
214   tissues for improved segmentation and evaluation of the tumor's extent. However, whenever a new
215   image is fed into the algorithm as input, post segmentation, the image is fed into the network's self-
216   learning layer as input for further images.

Self-Learning Network-Based Segmentation

218   In the automated segmentation of the brain MR image, the crucial thing is to set up training
219   sets that are large enough to train and validate the model. Resultantly it is challenging to obtain a
220   self-sufficient dataset for both trains and validating with ground facts that are associated with the
221   imaging data concerning to abnormality for cross validation. On the other hand, self-learning
222   models need a relatively smaller training and validation set. Furthermore, the experimental results
223   used in self-training the model ensure better results in future experimentation based on its previous
224   experimental knowledge. The complete flow diagram of the proposed framework can be seen in
225   figure 1 stated below.

226   **Figure 1** Represents the block diagram of SLNS based approach

Layered Architecture of SLNS

228   The layered architecture of the proposed Self-Learning Network-based Segmentation
229   (SLNS) approach includes the convolutional layers that would perform various challenging tasks
230   like pre-processing of the image to remove the image's noise by considering the adaptive bilateral
231   filter for pixels that surround the actual corresponding pixel. The image is then further processed
232   to remove the skull region in the next successive layer in correlation with the other connected
233   layers. Next, the image is segmented based on the pixel's intensity value, representing the region's
234   texture. And finally, the classifier is used to dissimilate the non-brain tissues and damaged Region
235   in the human brain.

236   The suggested methodology trains the segmentation algorithm using a self-learning module that
237   gets adequate information from the preset segmentation dataset and previous experimental results.
238   Additionally, each convolutional layer consists of a variety of kernels, including an adaptive
239   bilateral filter with sublayers that determine the appropriate number of clusters and cluster
240   centroids, Sobel filter that is used in the edge detection, and other 2D convolution filters that are
241   generally (3x3) in size which slides across the original input image. Over numerous epochs, the
242   model is trained over multiple iterations to identify all the key features in the input image. The
243   image is refined at the earlier stages using an Adaptive Bilateral filter that processes the image that
244   normalizes the noise like Gaussian noise and Poisson noise during image acquisition. The method
245   of noise reduction is carried forward through the following equations

246
$$AB_F = \alpha \times \Sigma_p p_b(||x - y||) \times p_l(||i_x - i_y||) \qquad (1)$$

247   From the above equation, the α value is determined by the contra harmonic mean of the
248   neighboring pixels determined in equation (2) stated below, Pb represents the pixel belongingness,
249   and p_l represents the pixel likeliness.

250
$$\alpha = \frac{i_1^2 + i_2^2 + i_3^2 + \dots + i_n^2}{i_1 + i_2 + i_3 + \dots + i_n} \qquad (2)$$

251   The values of the pixel belongingness (Pb) have been demonstrated in equation (3) mentioned
252   below

253
$$P_b = \frac{\Sigma_p c_p(p)^x p}{\Sigma_p c_p(p)^x} \qquad (3)$$

254   where cp determines the membership coefficient, and p designates the pixel, and x
255   designates the fuzzier metric of belongings. The value of the pixel likeliness(pl) is designated
256   through equation (4) stated below

257
$$p_l = p(s) \times p(\tfrac{cp}{s})/\Sigma p(k) \times p(\tfrac{cp}{k}) \qquad (4)$$

258   From the above equation, the p(s) denotes the probability of likeliness with the segment s,
259   and $p(\tfrac{cp}{s})$ represents the conditional probability concerning segment s and $\Sigma p(k) \times p(\tfrac{cp}{k})$ is
260   generally expected for all the classes.
261   Heuristic Approach for Real-time Image Segmentation (HARIS) algorithm is used to
262   segment the high dimensional images like the medical MR images to identify the abnormality from
263   the MR images. HARIS approach incorporates two phases in the image segmentation process. In
264   the initial phase, the optimal number of regions in the image are being assessed, which assists in
265   accurately recognizing the regions in the image based on texture, intensity, and boundary region-
266   related pixels. The techniques like the intraclass correlation and interclass variance are being
267   considered for evaluation. The second phase of the HARIS approach is to identify the local best
268   feature within the region following the presumed feature element that is presumed to be the global

269 best. The selected feature is being used in assembling the pixels as a region based on the feature
270 identified.
271   The image is segmented based on the intensity level in the later stages by approximating
272 the minimum number of segments to 23 from the previous experimental studies. The number of
273 segments fitness has been evaluated through the formula stated below

274
$$\text{Obj}_{\text{fun}} = \left(x \times \frac{\text{Tot}_{\text{pix}}}{\text{pix}_{\text{seg}}} \right) + \left(y \times \frac{T_s}{N_r} \right) \tag{5}$$

275   The above Equation (5), x, and y are the deciding factors that control the proposed
276 algorithm's accuracy and efficiency. x determines the inter-class variance, and y determines the
277 intraclass variance stated through equations (7) and (9).

278   The maximum interclass variance is being determined by the equation (6) stated below

279
$$\sigma^2\text{inter}_c(C_t) = \sigma^2\text{total}(C_t) - \sigma^2\text{prev\_inter}(C_t) \tag{6}$$

280
$$\sigma^2\text{inter}_c(C_t) = \sum_{x=0}^{C_t-1} p(x) \sum_{x=C_t}^{Z-1} p(x)[\mu_1(C_t) - \mu_2(C_t)]^2 \tag{7}$$

281   Equation (7) is the elaborated version of the equation (6) and Ct in the above equation
282 threshold value of the class that is being evaluated through the Fuzzy Entropy-based Thresholding
283 (FET) approach. And the variablesμ_1, μ_2 That determines the means of the intensities of the image
284 segment.
285   The fuzzy entropy-based (Oliva et al., 2019) thresholding technique that evaluates how
286 strongly a pixel is being strongly correlated to a particular segment, the value of the threshold is
287 being determined by the equation (8)

288 $\text{FET} = \sum_{\text{ints}=1}^{\max} \mu_{tc}(\text{ints})\log_2\mu_{tc}(\text{ints}) - \sum_{\text{ints}=\max+1}^{255} \mu_{ntc}(\text{ints})\log_2\mu_{ntc}(\text{ints}) \tag{8}$

289   From the above equation(8), the variables μ_{tc}, μ_{etc} Are the variables representing the fuzzy
290 membership concerning the image segments associated with the tumors class and non-tumors
291 class. However, the equation is formulated concerning Shannon's entropy formulation. And the
292 value of the threshold(FET) would be greater than 0 and would lie below 255.

293 The value of the intraclass correlation is determined by equation (9),

294
$$I_{\text{corl}} = \frac{\sigma_s^2}{\sigma_s^2 + \sigma_i^2} \tag{9}$$

295   From equation (9), the variable σ_s Represents the standard deviation in concern to the
296 given image segment, and the variableσ_i Represents the standard deviation concerning the entire
297 image that is being considered.

298 ***Adaptive Structural Similarity Index:***

299   The adaptive structural similarity index(ASSI) metric is used to classify the pixel among
300 the tumorous and non-tumorous regions. The structural similarity index relay on the likeness
301 among the pixels among tumor regions. The structural similarity index relies on three factors: the
302 structural parameter, luminance parameter, and contrast parameter. The index is determined as the

303   product of the three factors mentioned above. This paper has proposed an adaptive Structural
304   Similarity Index that would assess the membership alongside the similarity index to make the
305   outcome more realistic. The equation of the similarity index is determined through the equation
306   stated below

307
$$\text{ASSI}(p,q) = \omega \times \{x(p,q)\alpha.y(p,q)\beta.z(p,q)\gamma\} \quad (10)$$

308
$$x(p,q) = \frac{2\mu_p\mu_q + C_1}{\mu_p^2 + \mu_q^2 + C_1} \quad (11)$$

309
$$y(p,q) = \frac{2\sigma_p\sigma_q + C_2}{\sigma_p^2 + \sigma_q^2 + C_2} \quad (12)$$

310
$$z(p,q) = \frac{\sigma_{pq} + C_3}{\sigma_p\sigma_q + C_3} \quad (13)$$

311
$$\omega = \frac{\sigma_p^2}{(\sigma_p^2 + \frac{\sigma_e^2}{2})} \quad (14)$$

312   The equation (10) mentioned above is used to assess the likelihood of the pixel that could
313   be a part of the tumor region. The variable ω determines the probability that is multiplied by the
314   product of the structural parameter presented in equation (11), luminance parameter presented in
315   equation (12), and contrast parameter given in equation (13). The outcome of the proposed model
316   is promising when compared to that of its counterparts. The ASSI is used alongside the trained
317   models in the proposed self-learning model.

Algorithm

Date: x(p,q)←Structural Parameter, y(p,q)←Luminance Parameter, z(p,q)← Contrast Parameter
Input: pixel(p,q) where p represents the row and the q represents the column
Output: Assess the correlation index
 	
pix(p,q)← initialize the starting pixel
while(i<maximum_number_iterations)
    for each pixel in the input image, **do**
    Update x(p,q), y(p,q), z(p,q) and ω
       Approximate the **Correlation Index**
          Select the regions in the image
          Determine the suitable category to assign
            If CI > Threshold, **then**
              Assign the corresponding pixel to the tumorous Region
          else
              Assign the corresponding pixel to the non-tumorous Region
          end if
    end for
end While

318

319   Figure 2 represents the proposed model's layered architecture. The convolutional layer,
320   max-pool layer, flattening layer, and fully connected layers almost resemble the Convolutional

321 Neural Network model (Farhana et al., 2020). The Convolutional layer in the proposed architecture
322 is responsible for applying kernels' sequence to the input MR images for extracting the features
323 from the image that assist in classifying various regions in the input image. The convolution layer
324 identifies the pixels' spatial association based on the selected features informing the Region,
325 making abnormality identification easy. The pooling layer is generally next to the convolution
326 layer, which is meant for reducing the special size of the outcome in the previous layer, which
327 would resultantly minimize the number of parameters and features that are deliberated for further
328 processing and to minimize the computational time. In the proposed model, the MAX pooling
329 approach is considered in reducing the spatial size. Convolution and Max Pooling layers are used
330 concurrently for numerous rounds until all regions are well-tuned, and features are recognized.

331   **Figure 2** Architecture diagram of the proposed SLNS model

332   The flattening layer is the successive layer after the Convolution and Pooling layers. It is
333 responsible for transferring the data into the 1-dimensional array used in the subsequent layered
334 architecture. The Fully Connected layer in the proposed architecture uses the intensity features of
335 the regions that are recognized as abnormal and normal in the considered MR images. Gated
336 Recurrent Unit (GRU) is being used in the proposed model to maintain the interpreted data of the
337 previous experimental prediction. The same apprehension is being used in the future in
338 abnormality recognition from the MR Image. Heuristic Approach for Real-time Image
339 Segmentation (HARIS) algorithm is being used to differentiate the tumors and non-tumors Region
340 by identifying the appropriate pixels as the features for the prediction.

341   The Gated Recurrent Unit is used to maintain the acquired knowledge from the previous
342 outcomes. GRU is efficient, with comparatively fewer parameters needed to maintain the training
343 data, (Guizhu et al., 2018) (Le et al., 2016). GRU can address challenging tasks like vanishing
344 gradient problems through the two gates, namely the reset gate and the update gate. HARIS works
345 with both the fully connected and GRU layers to recognize the suitable pixels for the prediction.
346 The cost function of the proposed model in concern to the tensors for the input image I(i,j) can be
347 evaluated through the equation (15)

348 $$j(w,\beta;i,j) = \frac{\|f_{w,\beta}(i) - j\|^2}{2} \qquad (15)$$

349   The variable w represents the weight associated with layer l and the variable β represents
350 the bias, $f_{w,\beta}(i)$ represents the kernel that is being used in operating the elements. The error at the
351 layer l in the proposed model is determined through the equation (16)

352 $$e^l = ((w^l)^t e^{l+1}) \cdot f(x^l) \qquad (16)$$

353   The w^l is the weight that is associated with layer l and the variable e^{l+1} represents the
354 error associated with layer $l + 1$. The variable $f(x^l)$ is the activation function that is associated
355 with the layer l that is being determined by the Rectified Linear Unit (ReLu) in the proposed model.

356 $$ReLu(x^l) = max(0,x) \qquad (17)$$

357   The ReLu based activation function is linear for the greater than zero values, and it will be
358 zero for all the negative values.

359   The learning rate of the proposed model is significant in assessing the performance of the
360   model, which generally controls the weights in the network in concern to the loss gradience. The
361   learning rate is presumed to be at an optimal level so that the model will move towards the solution
362   by considering all the significant features in the prediction. The lesser learning rate presents the
363   slower learning ability resulting in a delayed solution. On the other hand, the higher learning rate
364   results in a faster solution that may ignore few features in the learning process. Figure 3 represents
365   the learning rate of the proposed model across various epochs. Initially with fewer epochs the
366   learning rate of the model is high that implies the model is learning faster from the training data
367   and as we increase the epochs the learning rate is saturated that implies the model is learning only
368   the new insights from the training data, the same scenario can be observed from figure 3. The
369   saturation point for the learning rate in the proposed model is achieved at the epoch=43 and the
370   iteration=187.
371
372   **Figure 3** The graph representing the Learning Rate
373   In the proposed self-learning centric segmentation model, the model will acquire
374   knowledge from the earlier experimental outcomes. The learning rate is also dependent on the
375   number of epochs that the model is designed to execute before it is evaluated. As the number of
376   epochs increases, the learning rate of the model will move towards the saturation point, and we
377   can observe the change in the learning rate till that point. But increasing the number of epochs will
378   result in consuming more computational efforts in the training process.
379   The other hyperparameters associated with the evaluation process include the loss and
380   accuracy functions related to the proposed model's training and validation phase. It can be seen
381   from Figure 4, the left side graph represents the training, and the validation loss of the model,
382   wherein graph after a certain number of epochs, approximately from 15, the training and the
383   validation loss are close to each other, that determines the proposed model is reasonably good in
384   identifying the abnormalities from the MR images. When the validation loss is much higher than
385   the training loss, it is assumed as the overfitting, which results in incorrect classification of the
386   abnormal region. Underfitting is a situation in which the training loss is more than the validation
387   loss that would result in poor accuracy of the model due to inappropriate selection of the features
388   in the data. Thus, training and validation accuracy are the other parameters that are considered for
389   evaluating the proposed model. The graph that is on the right side represents the accuracy measures
390   of the proposed model.
391
392   **Figure 4** The image representing the hyper-parameters

393   **Experimental Results And Observations**

394   The experimentation has been carried forward over the real-time MR images acquired from
395   the open-source repository LGG dataset acquired from The Cancer Genome Atlas (TCGA)
396   captured from patients with acute glioma. The performance of the proposed approach has been
397   evaluated through various metrics like Sensitivity, Specificity, Accuracy, Jaccard Similarity Index,

398   and Matthews Correlation Coefficient that is being assessed from the True Positive value that
399   designates how many times does the proposed approach correctly recognize the damaged Region
400   in the human brain as damaged Region and the True Negative that designates the how many times
401   the proposed approach identifies non-damaged Region correctly and False Positive designates the
402   number of times does the proposed approach identifies damaged Region in the brain as non-
403   damaged Region and False Negative designate the count of how many times does the proposed
404   approach mistakenly chosen non- tumors region as tumors region. Figure 5 presents the output
405   screens of the proposed model.

406

407   **Figure 5** Output screens of proposed SLNS approach

408   The performance of the proposed Self-Learning Network-based Segmentation (SLNS)
409   approach is being evaluated against the other conventional approaches like Twin-Centric GA with
410   SGO, HARIS approach, and Convolutional Neural Network in concern to the performance
411   evaluation metrics like Sensitivity, Specificity, Accuracy, Jaccard Similarity Index (JSI), Mathew
412   Correlation Coefficient(MCC). Table 1 represents the experimental evaluations of the proposed
413   model. The experimentation is conducted by executing the code repeatedly 35 times and scaled up
414   for evaluating the confusion matrix. The model's accuracy is assessed with a standard deviation of
415   ±0.015 in assessing the segmented image as a present by (Agrawal et al., 2019).

416

417   **Table 1.** The table represents the confusion matrix of the proposed model

418

419   **Table 2.** Performance analysis of the proposed approach

420

421   From table 2, it is observed that the proposed SLNS approach is outperforming when
422   compared to its counterparts. In many of the cases, the proposed approach seems much better than
423   CNN. The semi-trained approach needs comparatively fewer efforts than CNN at the same
424   performance. And in the computational efforts perspective, the proposed algorithms need almost
425   the same execution time as the CNN algorithm but more time than the HARIS Algorithm-based
426   segmentation approach. Fuzzy entropy-based MR image segmentation as experimented by
427   (Rajinikanth & Satapath, 2018), (Chao et al., 2016). Figure 6 presents the comparative analysis of
428   the various approaches.

429

430   **Figure 6.** Graph representing the comparative analysis of various approaches

431   The performance of the proposed model is being assessed through the HARIS algorithm
432   that decides the best possible number of segments to assist in identifying the abnormalities in the
433   image, and it assigns the pixels to the segment by identifying the ideal pixel in the segment. The
434   second objective function of the HARIS algorithm is being replaced with the fuzzy membership
435   assessment model, and the performance of the proposed model is being evaluated and presented
436   in table 3. The fuzzy membership is evaluated through equation (15) stated by (Vaidya et al.,
437   2018). The membership is evaluated as follows

438   $$membership = \ vertex_{pix} - \frac{vertex_{pix} - I'_{pix}}{1 - mem_{pix}(I'_{pix})} \qquad (18)$$

439   From equation(15), the variable$vertex_{pix}$ represents the vertices that are being considered
440 in the image for processing. The variable I'_{pix} represents the instance data that are the pixels, and
441 the variable $mem_{pix}(I'_{pix})$ presents the minimum correlation value in concern to the MR image
442 segment. The segment vertex is being assessed through the equation(16) stated below

443 $$vertex = vertex_{pix} + \frac{J'_{pix} - vertex_{pix}}{1 - mem_{pix}(J'_{pix})} \qquad (19)$$

444   From equation(16), $vertex_{pix}$ represents the vertex pixel in the region of the MR image.
445 The variable J'_{pix} represents the instance pixel in the segment and$mem_{pix}(J'_{pix})$ represents the
446 membership value. It can be observed from table 3. Thus, the fuzzy membership-based HARIS
447 algorithm has slightly performed well than the traditional HARIS algorithm.

448

449   **Table 3**. Table representing the performance analysis with Fuzzy Component

450

451   **Figure 7.** Graph representing the computational time of various approaches

452   Figure 7 presents the assessed computational time consumed by various algorithms. It
453 could be observed from the graphical values that the proposed approach SLNS seems to be much
454 efficient. It is observed that SLNS consumes more time than the HARIS-based approach, but from
455 a precision point of view, the proposed SLNS has a trade-off. The computational time of CNN and
456 SLNS is almost the same, and the computational lag in the proposed approach is because of self-
457 training that needs additional efforts. The proposed model does not require any significant training,
458 unlike the neural network-based models.

459

460   The proposed model's performance is assessed against the various existing algorithms like
461 thresholding, Seeded Region Growing, Fuzzy C-Means, and the Artificial Neural Network models
462 concerning the evaluation metrics like sensitivity, specificity, and accuracy presented by (Alam et
463 al., 2019). The comparative analysis of the approaches with obtained values is shown in table 4.
464 The performances of various algorithms connected to the proposed SLNS have been assessed
465 concerning the size of the tumor. It is observed that from the clinical evidence, the resultant
466 outcomes have been proven to be better compared to their counterparts and the consequent of the
467 proposed methods seems to very pleasing and very accurate. The tabulated values in table 4
468 represent the resultant experimental values.

469

470   **Table 4.** Table representing the performance analysis of SLNS approach

471   Table 4 represents the progress of the tumor growth, that is being identified based on the
472 texture information of the abnormal region as stated by (Naga et al., 2020). The abnormal region
473 is classified as the Tumour Core(TC) that depicts the actual region of the tumor, and the Enhanced
474 Tumour(ET) that depicts the recent enhancement that has taken place in the region of the tumor
475 that is presumed to be the progress in the tumor. The Whole Tumour(WT) is the region that
476 includes both the tumor core and the enhanced tumor regions. The enhanced tumor region presents
477 the progress of the abnormality that will assist the physician in taking up the decisions for suitable
478 treatment.

479    The self-learning-centric models are recently becoming part of the biomedical and
480 healthcare domain, where the models are expected to work with minimal training. In a few
481 situations where there is no adequate data available for training the model, the self-learning models
482 are proven to perform well. The model also needs lesser training than its counterparts. The
483 proposed model is capable of learning from its previous experimental results. The hyperparameters
484 like the learning rate that are presented in the current study are at an acceptable level after 43
485 epochs, and other parameters like the training and validation studies state that the model fine-tuned
486 The performance assessment metrics like the accuracy, sensitivity, specificity, Jaccard Similarity
487 Index (JSI), Mathew Correlation Coefficient(MCC) are assessed by repeated autonomous
488 executions. The obtained values have proven that the model performs reasonably with minimal
489 training of the data. The fuzzy component is being added to evaluate the membership for assigning
490 the pixels to the appropriate segment in contrast to the HARIS algorithm for the assignment of the
491 pixels. The statistical analysis of the study has evinced the performance of the HARIS algorithm
492 in the segmentation process.

Conclusions

494    The pivotal object of the current study on mechanizing a self-learning model that is
495 efficient in identifying the tumor from the MR image with minimal training. The model is efficient
496 in working with problems that have minimal training data available. The proposed model
497 efficiently learns from its prior experimental outcomes and utilizes the acquired knowledge for
498 future predictions. It is observed on the practical implementation of the proposed model that the
499 resulting outcome seems to be much accurate and precise in identifying abnormality in the human
500 brain. In contrast to fully supervised models like Convolutional Neural Networks, deep learning
501 models and various classification algorithms need to be rigorously trained for better accuracy. Still,
502 the proposed model is proven to be efficient in generating equivalently better outcomes with other
503 models. The proposed model itself can normalize the noise in the input image and robust in
504 differentiating the non-brain tissues like the skull from the brain tissues. However, the proposed
505 approach could be further optimized by incorporating the self-correcting convolution layer through
506 an Ancillary kernel.

507    The self-Learning models are robust in handling the unusual problem where there is
508 inadequate training data available. But the self-learning models overfit in few cases as the
509 developer may not have control over the level of training to the model. The overfitting may lead
510 to instability in the predictions that are made in few contexts. Moreover, the process of debugging
511 the issues and rectifying them in the self-learning model is challenging. The models learn from
512 their previous experimental outcomes, and there is a possibility that the models might misinterpret
513 the outcome based on previous experimental results.

Future Scope

515 The proposed model based on the self-learning mechanism is suitable for handling uncertain data
516 more effectively through its previous experiences. The model's performance can be further
517 improvised by incorporating the Long Short Term Memory(LSTM) component for efficiently
518 handling the training data for better accurate prediction of the progress in the tumor growth as the
519 LSTM components are efficient in holding the memories for a longer time by preserving the
520 dependencies based on the network's information. The incorporated memory elements can retain
521 the State information over the specific iterations constructed through multiple gates. The proposed

522 model can also be enhanced by incorporating the feedback component that would help assess
523 tumor growth progress by correlating its previous outcome.

524

Availability of Dataset

526 The datasets used for the experimental purpose are open available over the web with the ground
527 facts that will support evaluating the performance of the proposed model. TCGA-LGG dataset can
528 be downloaded from the website https://wiki.cancerimagingarchive.net/display/Public/TCGA-
529 LGG, and the dataset related to the experimentation is openly available at
530 https://www.kaggle.com/mateuszbuda/lgg-mri-segmentation/version/1.

531

References

533

534 Agrawal R, Sharma M, Bikesh KS. 2019. Segmentation of Brain Tumour Based on Clustering
535   Technique: Performance Analysis. *Journal of Intelligent Systems,* vol. 28, no. 2, pp. 291-
536   306. https://doi.org/10.1515/jisys-2017-0027

537 Al-Shamasneh AR, Jalab HA, Shivakumara P, Ibrahim RB, Obaidellah U. 2020. Kidney
538   segmentation in MRI images using active contour model driven by fractional-based energy
539   minimization. *Signal Video and Image Processing*, vol.14, Pp. 1361–1368.
540   https://doi.org/10.1007/s11760-020-01673-9.

541 Alam MS, Rahman MM, Hossain MA, Islam MK, Ahmed KM, Ahmed KT, Singh BC, Miah MS.
542   2019. Automatic Human Brain Tumor Detection in MRI Image Using Template-Based K
543   Means and Improved Fuzzy C Means Clustering Algorithm. *Big Data and Cognitive
544   Computing*, Vol. 3(2):27. https://doi.org/10.3390/bdcc3020027

545 Bal A, Banerjee M, Sharma P, Maitra M. 2018. Brain Tumor Segmentation on MR Image Using
546   K-Means and Fuzzy-Possibilistic Clustering. 2018 2nd International Conference on
547   Electronics, Materials Engineering & Nano-Technology (IEMENTech), pp. 1-8, doi:
548   10.1109/IEMENTECH.2018.8465390.

549 Chahal PK, Pandey S, Goel S. 2020. A survey on brain tumor detection techniques for MRI
550   images. *Multimedia Tools Applications*, Vol. 79, pp. 21771–21814.
551   https://doi.org/10.1007/s11042-020-08898-3

552 Chao Y, Dai M, Chen K, P. Chen and Z. Zhang. 2016. Fuzzy entropy based multilevel image
553   thresholding using modified gravitational search algorithm. 2016 *IEEE International
554   Conference on Industrial Technology (ICIT)*, Taipei, Taiwan, pp. 752-757, doi:
555   10.1109/ICIT.2016.7474845.

556 Dalvand M, Fathi A, Kamran A. 2020. Flooding region growing: a new parallel image
557   segmentation model based on membrane computing. *Journal of Real-Time Image
558   Proceedings*. https://doi.org/10.1007/s11554-020-00949-0

559 De, Guo C. 2015. An adaptive vector quantization approach for image segmentation based on
560   SOM network, *Neurocomputing* 198, pp 48–58.

561 Deepalakshmi P, Krishna TP, Chandana SS, Lavanya K, Srinivasu PN. 2021. Plant Leaf Disease
562   Detection Using CNN Algorithm. *International Journal of Information System Modeling
563   and Design*, Vol. 12(1), pp. 1-21. doi:10.4018/IJISMD.2021010101

564 Dey N, Rajinikanth V, Ashour AS, Tavares JMRS. 2018. Social Group Optimization Supported
565   Segmentation and Evaluation of Skin Melanoma Images. *Symmetry*. Vol. 10(2):51.
566   https://doi.org/10.3390/sym10020051

567 Diaz I, Boulanger P. 2015. Atlas to Patient Registration with Brain Tumor Based on a Mesh-free
568   Method. Conference proceedings: Annual International Conference of the IEEE Engineering
569   in Medicine and Biology Society. *IEEE Engineering in Medicine and Biology Society*.
570   Conference. 2015. 10.1109/EMBC.2015.7319004.

571 Farhana S, Abu S, Paramartha D. 2020. Evolution of Image Segmentation using Deep
572   Convolutional Neural Network: A Survey, *Knowledge-Based Systems*, Vol. 201–202, pp.
573   106062,ISSN 0950-7051,https://doi.org/10.1016/j.knosys.2020.106062.

574 Gibran MK, Nababan EB, Sihombing P. 2020. Analysis of Face Recognition with Fuzzy C-Means
575   Clustering Image Segmentation and Learning Vector Quantization. *3rd International
576   Conference on Mechanical, Electronics, Computer, and Industrial Technology (MECnIT),
577   Medan, Indonesia*, pp. 188-193, doi: 10.1109/MECnIT48290.2020.9166649.

578 Guizhu S, Qingping T, Haoyu Z, Ping Z, Jianjun X. 2018. Deep Learning with Gated Recurrent
579   Unit Networks for Financial Sequence Predictions, *Procedia Computer Science*, Vol. 131,
580   Pp. 895-903,ISSN 1877-0509.

581 Havaei M, Davy A, Farley DW, Biard A,Courville A, Bengio Y, Pal C, Jodoin PM, Larochelle H.
582   2016. Brain tumor segmentation with Deep neural networks, *Medical Image Analysis*. Vol
583   35 ,pp. 18–31. https://doi.org/10.1016/j.media.2016.05.004

584 Javaria A, Muhammad S, Mudassar R, Tanzila S, Muhammad AA. 2019. Brain tumor detection
585   using statistical and machine learning methods. *Computer Methods and Programs in
586   Biomedicine*. Vol. 177, pp. 69-79.

587 Jude DH, Anitha J, Balas VE. 2015. Performance Improved Modified Fuzzy C-Means Algorithm
588   for Image Segmentation Applications. *Informatica*. Vol. 26. Pp. 635-648.
589   10.15388/Informatica.2015.68.

590 Kornilov A, Safonov I. 2018. An Overview of Watershed Algorithm Implementations in Open
591   Source Libraries. *Journal of Imaging*. Vol. 4(10):123. 10.3390/jimaging4100123.

592 Kumar R, Talukdar F, Dey N, Ashour AS, Santhi V, Balas V, Fuqian S. 2015. Histogram
593   Thresholding in Image Segmentation: A Joint Level Set Method and Lattice Boltzmann
594   Method based Approach.

595 Le T, Kim J, Kim H. 2016. Classification performance using gated recurrent unit recurrent neural
596   network on energy disaggregation. *International Conference on Machine Learning and
597   Cybernetics (ICMLC)*, Jeju, 2016, pp. 105-110, doi: 10.1109/ICMLC.2016.7860885.

598 Li Y, Liang W, Zhang Y, Tan J. 2018. Automatic Global Level Set Approach for Lumbar
599   Vertebrae CT Image Segmentation. *BioMed Research International*. pp.1-12.
600   10.1155/2018/6319879.

601 Liang Y, Fu J. 2018. Watershed Algorithm for Medical Image Segmentation Based on
602   Morphology and Total Variation Model. *International Journal of Pattern Recognition and
603   Artificial Intelligence*. 33. 10.1142/S0218001419540193.

604 Liu Z, Li X, Luo P, Loy CC, Tang X. 2018. Deep Learning Markov Random Field for Semantic
605   Segmentation. *In IEEE Transactions on Pattern Analysis and Machine Intelligence*, vol.
606   40(8), pp. 1814-1828, DOI: 10.1109/TPAMI.2017.2737535.

607   Madallah A, Muhammad HS, Muhammad AJ. 2020. A robust clustering algorithm using spatial
608   fuzzy C-means for brain MR images, *Egyptian Informatics Journal*, Vol. 21(1), pp. 51-66,
609   https://doi.org/10.1016/j.eij.2019.10.005.

610   Mathur N, Mathur S, Mathur D. 2016. A novel approach to improve Sobel Edge detector, In
611   Proceedings of the 6th International Conference on Advances in Computing and
612   Communications, India, *Procedia Computer Science*, Pp. 431– 438.

613   Misra I, Zitnick C, Mitchell M, Girshick R. 2016. Seeing through the Human Reporting Bias:
614   Visual   Classifiers   from   Noisy   Human-Centric   Labels.   Pp.   2930-2939.
615   10.1109/CVPR.2016.320.

616   Norbert G, Ian L, Pope BW, Javier A, Karl-Josef L. 2017. The use of amino acid PET and
617   conventional MRI for monitoring of brain tumor therapy, *NeuroImage: Clinical*, Vol. 13,
618   pp. 386-394. https://doi.org/10.1016/j.nicl.2016.12.020.

619   Oliva D, Elaziz AM, Hinojosa S. 2019. Fuzzy Entropy Approaches for Image Segmentation. In:
620   Metaheuristic Algorithms for Image Segmentation: Theory and Applications. *Studies in*
621   *Computational Intelligence*, vol 825. Springer, Cham. https://doi.org/10.1007/978-3-030-
622   12931-6_11

623   P.A. Mei, C.C. Carneiro, S.J. Fraser, L.L. Min, and F. Rels. 2015. Analysis of neoplastic lesions
624   in magnetic resonance imaging using self-organizing maps, *Journal Neurological*
625   *Sciences*.359 ,pp. 78–83.

626   Pandav   S.   2014. Brain   tumor   extraction   using   marker   controlled   watershed
627   segmentation, *International Journal of Engineering Research and Technology*, Vol. 3(6).
628   ISSN: 2278-0181.

629   Punitha S, Amuthan A, Joseph KS. 2018. Benign and malignant breast cancer segmentation using
630   optimized Region growing technique, *Future Computing and Informatics Journal*, Vol. 3(2),
631   pp. 348-358. https://doi.org/10.1016/j.fcij.2018.10.005.

632   Qayyum, Huma & Majid, Muhammad & Anwar, Syed. 2017. Facial Expression Recognition
633   Using Stationary Wavelet Transform Features. *Mathematical Problems in Engineering*. pp.
634   1-9. 10.1155/2017/9854050.

635   Rajinikanth V, Satapathy SC. 2018. Segmentation of Ischemic Stroke Lesion in Brain MRI Based
636   on Social Group Optimization and Fuzzy-Tsallis Entropy. *Arabian Journal for Science and*
637   *Engineering* 43, 4365–4378. https://doi.org/10.1007/s13369-017-3053-6

638   Sachdeva J, Kumar V, Gupta I, Khandelwal N, Ahuja CK. 2016. A package-SFERCB-
639   Segmentation, feature extraction, reduction, and classification analysis by SVM and ANN
640   for   brain   tumors. *Applied   Soft   Computing*,   Vol. 47, pp.   151–167.
641   https://doi.org/10.1016/j.asoc.2016.05.020

642   Sandhya G, Babu KG, Satya TS. 2020. Tumor Segmentation by a Self-Organizing-Map based
643   Active   Contour   Model   (SOMACM)   from   the   Brain   MRIs, *IETE   Journal   of*
644   *Research*, DOI: 10.1080/03772063.2020.1782780

645   Schillaci O, Urbano N. 2019. Digital PET/CT: a new intriguing chance for clinical nuclear
646   medicine and personalized molecular imaging. *European Journal of Nuclear Medicine and*
647   *Molecular Imaging*. Vol. 46, pp. 1222–1225. https://doi.org/10.1007/s00259-019-04300-z.

648   Sheela CJJ, Suganthi G. 2020. Morphological edge detection and brain tumor segmentation in
649   Magnetic Resonance (MRI) images based on region growing and performance evaluation of
650   modified Fuzzy C-Means (FCM) algorithm. *Multimedia Tools and Applications*.*Vol.* 79,

651	pp. 17483–17496. https://doi.org/10.1007/s11042-020-08636-9

652	SivaSai JG, Srinivasu PN, Sindhuri MN, Rohitha K, Deepika S. 2021. An Automated
653	Segmentation of Brain MR Image Through Fuzzy Recurrent Neural Network. In: Bhoi A.,
654	Mallick P., Liu CM., Balas V. (eds) Bio-inspired Neurocomputing. *Studies in Computational*
655	*Intelligence,* vol 903. Springer, Singapore. https://doi.org/10.1007/978-981-15-5495-7_9

656	Sowjanya K, Rajesh KP, Satish KI. 2018. Optimal multilevel thresholding selection for brain MRI
657	image segmentation based on adaptive wind-driven optimization, *Measurement*, Vol. 130,
658	Pages 340-361. https://doi.org/10.1016/j.measurement.2018.08.007.

659	Srinivasu PN, Rao TS, Dicu AM, Mnerie C, Olariu I. 2020. A comparative review of optimisation
660	techniques in segmentation of brain MRI images. *Journal of Intelligent & Fuzzy Systems.*
661	Vol. 38, pp. 1-12, 10.3233/JIFS-179688.

662	Srinivasu PN, Rao TS, Balas, VE. 2020. A systematic approach for identification of tumor regions
663	in the human brain through HARIS algorithm. In: Deep Learning Techniques for Biomedical
664	and Health Informatics, pp. 97–118. *Academic Press.* https://doi.org/10.1016/B978-0-12-
665	819061-6.00004-5.

666	Srinivasu PN, Rao TS, Balas, VE. 2020. Volumetric Estimation of the Damaged Area in the
667	Human Brain from 2D MR Image. *International Journal of Information System Modeling*
668	*and Design* (IJISMD), 11(1), 74-92. doi:10.4018/IJISMD.2020010105

669	Srinivasu PN, Rao TS, Srinivas G, Reddy PVGDP. 2020. A Computationally Efficient Skull
670	Scraping Approach for Brain MR Image. *Recent Advances in Computer Science and*
671	*Communications*13: 833. https://doi.org/10.2174/2213275912666190809111928

672	Srinivasu PN, SivaSai JG, Ijaz MF, Bhoi AK, Kim W, Kang JJ. 2021. Classification of Skin
673	Disease Using Deep Learning Neural Networks with MobileNet V2 and LSTM. *Sensors*,
674	Vol. 21(8):2852. https://doi.org/10.3390/s21082852

675	Sudharania K, Sarma TC, Prasad KS. 2016. Advanced morphological technique for automatic
676	brain tumor detection and evaluation of statistical parameters, *Procedia Technology*.
677	Vol. 24, pp. 1374– 1387.

678	Vaga R, Bryant K. 2016. Recent advances in x-ray technology, *2016 Pan Pacific Microelectronics*
679	*Symposium (Pan Pacific), Big Island*, HI, pp. 1-10. DOI: 10.1109/PanPacific.2016.7428397.

680	Vaidya AV, Metkewar PS, Naik SA. 2018. A New Paradigm For Generation Of Fuzzy
681	Membership Function. 2018 IEEE 8th International Advance Computing Conference
682	(IACC), Greater Noida, India, pp. 1-6, doi: 10.1109/IADCC.2018.8692089.

683	Varuna NS, Kumar TNR. 2018. Identification and classification of brain tumor MRI images with
684	feature extraction using DWT and probabilistic neural networks. *Brain Informatics*. Vol.
685	5, pp. 23–30. https://doi.org/10.1007/s40708-017-0075-5

686	Venkatesan V, Sandhya M., Jenefer B. 2017. Computed tomography scan simulation techniques:
687	A survey. *2017 Fourth International Conference on Signal Processing, Communication and*
688	*Networking (ICSCN), Chennai*, pp. 1-5.

689	Venmathi AR, Ganesh EN, Kumaratharan N. 2019. Image Segmentation based on Markov
690	Random Field Probabilistic Approach. *2019 International Conference on Communication*
691	*and Signal Processing (ICCSP),* Chennai, India, pp. 0490-0495, DOI:
692	10.1109/ICCSP.2019.8697912.

693   Verma H, Agrawal RK, Sharan A. 2015. An improved intuitionistic fuzzy c-means clustering
694   algorithm incorporates local information for brain image segmentation, *Applied Soft*
695   *Computing*. Vol. 46, pp. 543–557.

696   Wang M, Li P, Liu F. 2019. Multi-atlas active contour segmentation method using a template
697   optimization algorithm. *BMC Med Imaging*. Vol. **19(**42). https://doi.org/10.1186/s12880-
698   019-0340-6

699   Wentao W, Daning L, Jiaoyang D, Xiangyu G, Wen G, Fanfan Z, Xiaojie F, Hong Y. 2020. An
700   Intelligent Diagnosis Method of Brain MRI Tumor Segmentation Using Deep Convolutional
701   Neural Network and SVM Algorithm. *Computational Intelligence Methods for Brain-*
702   *Machine Interfacing or Brain-Computer Interfacing*, Volume 2020, Article ID 6789306,
703   https://doi.org/10.1155/2020/6789306

704   Xiao T, Xia T, Yang Y, Huang C, Wang X. 2015.Learning from massive noisy labeled data for
705   image classification. *EEE Conference on Computer Vision and Pattern Recognition (CVPR)*,
706   Boston, MA, pp. 2691-2699, DOI: 10.1109/CVPR.2015.7298885.

Figure 1

Represents the block diagram of SLNS based approach
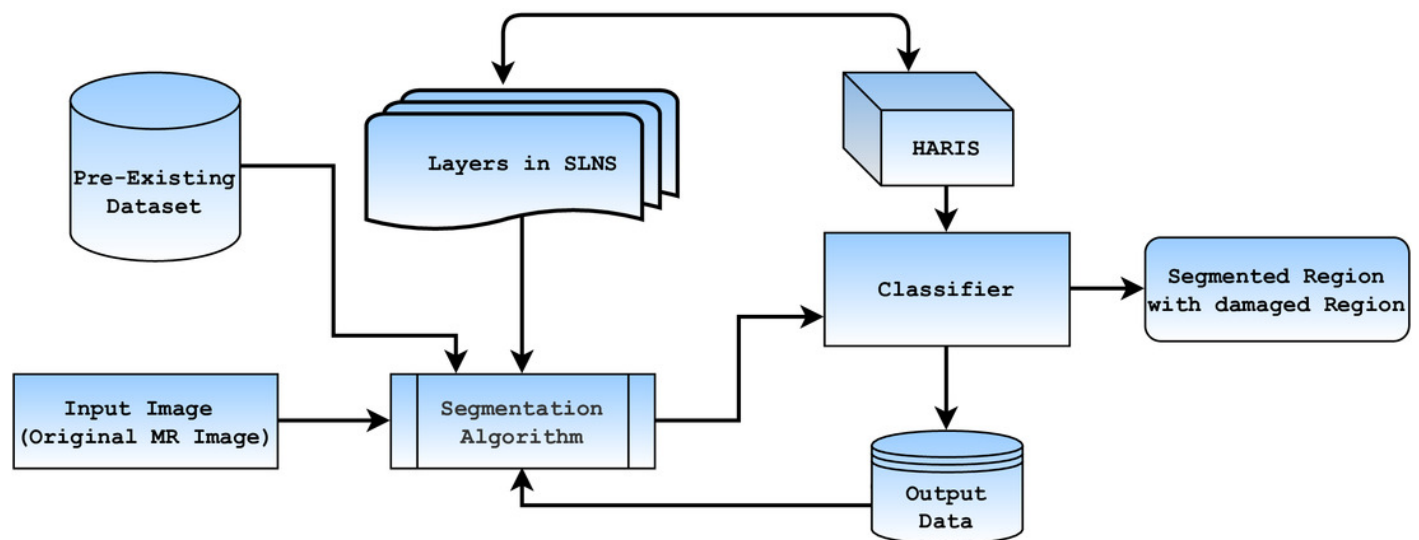
Figure 2

Architecture diagram of the proposed SLNS model
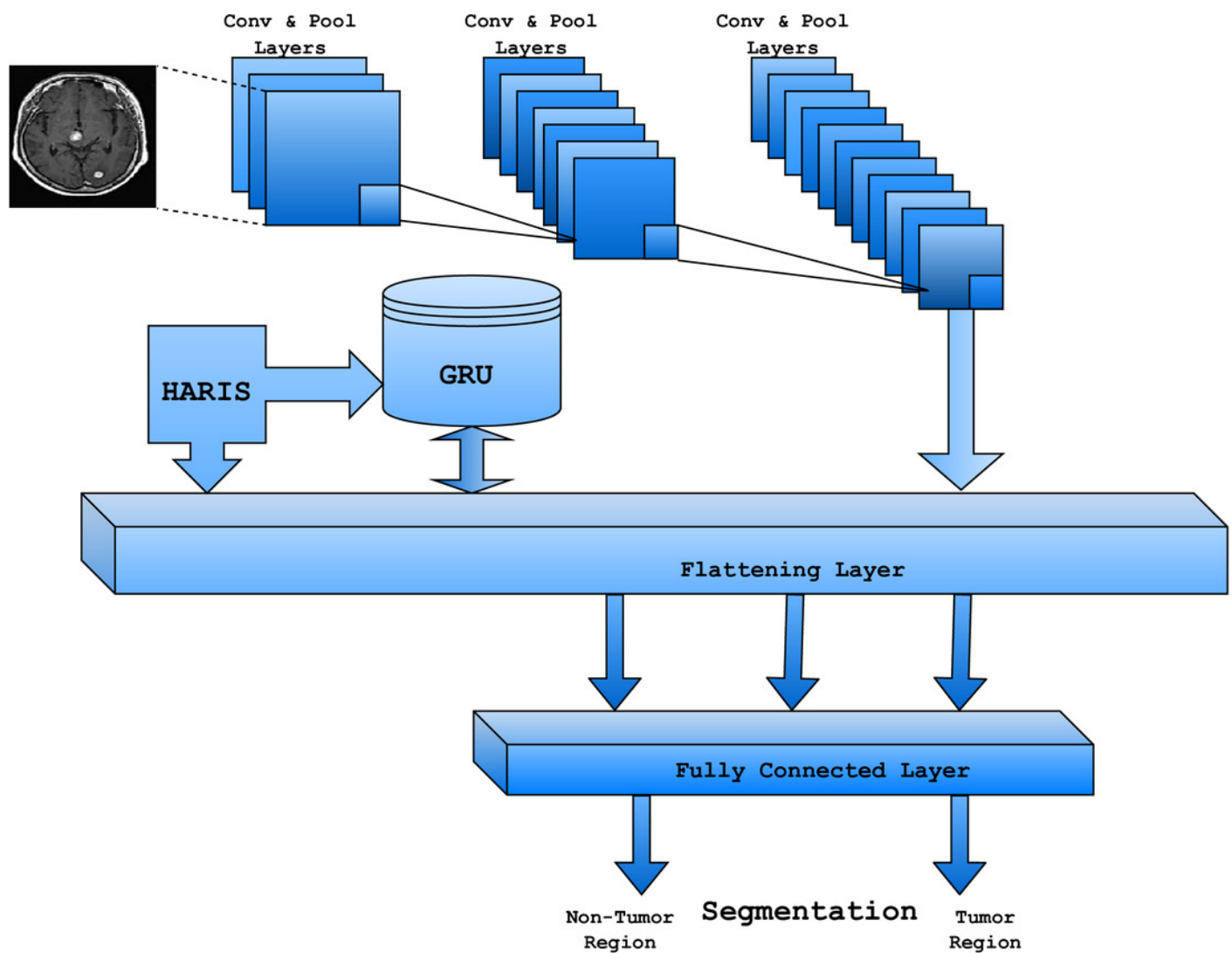
Figure 3

The graph representing the Learning Rate
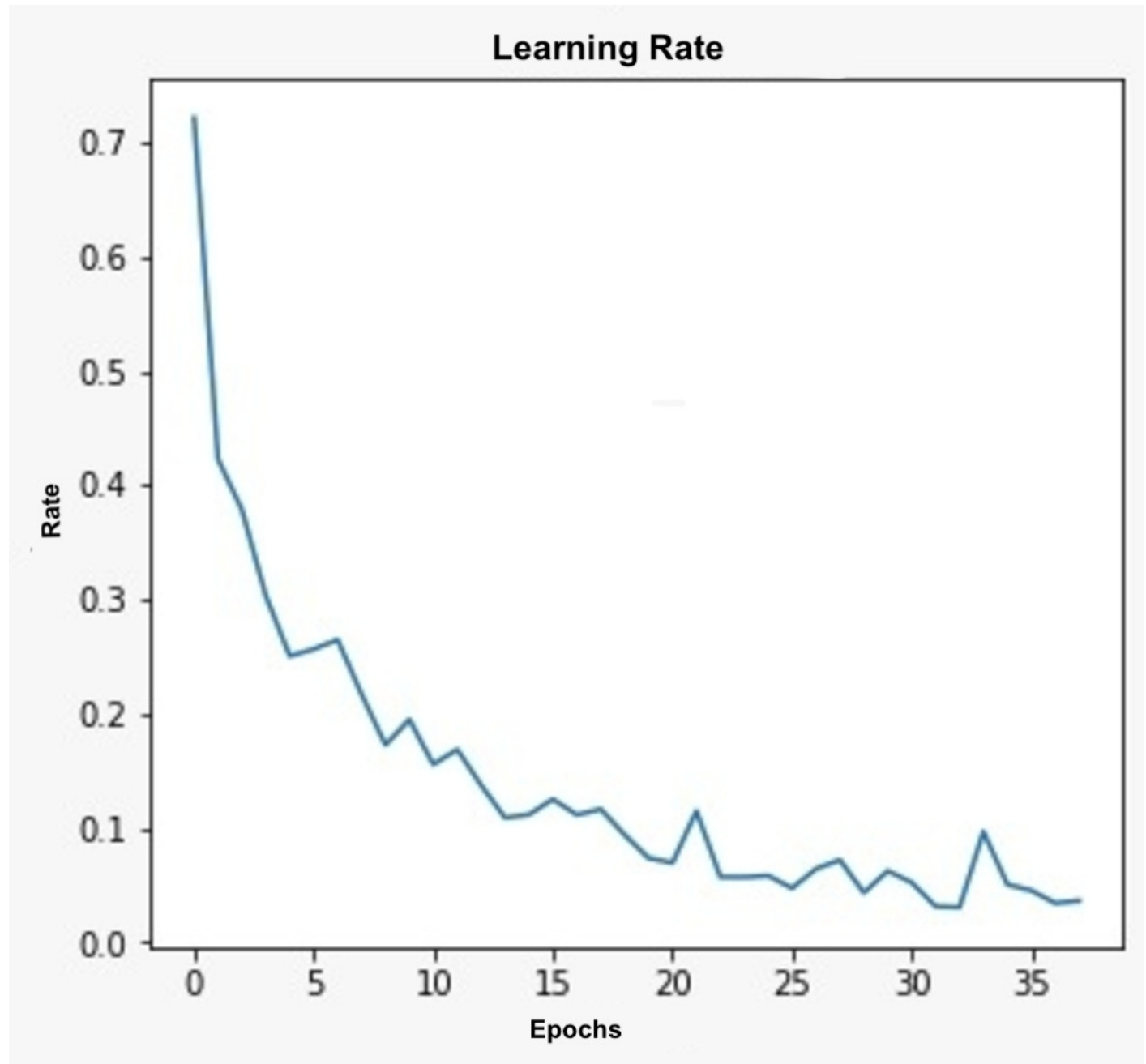
Figure 4

The image representing the hyper-parameters
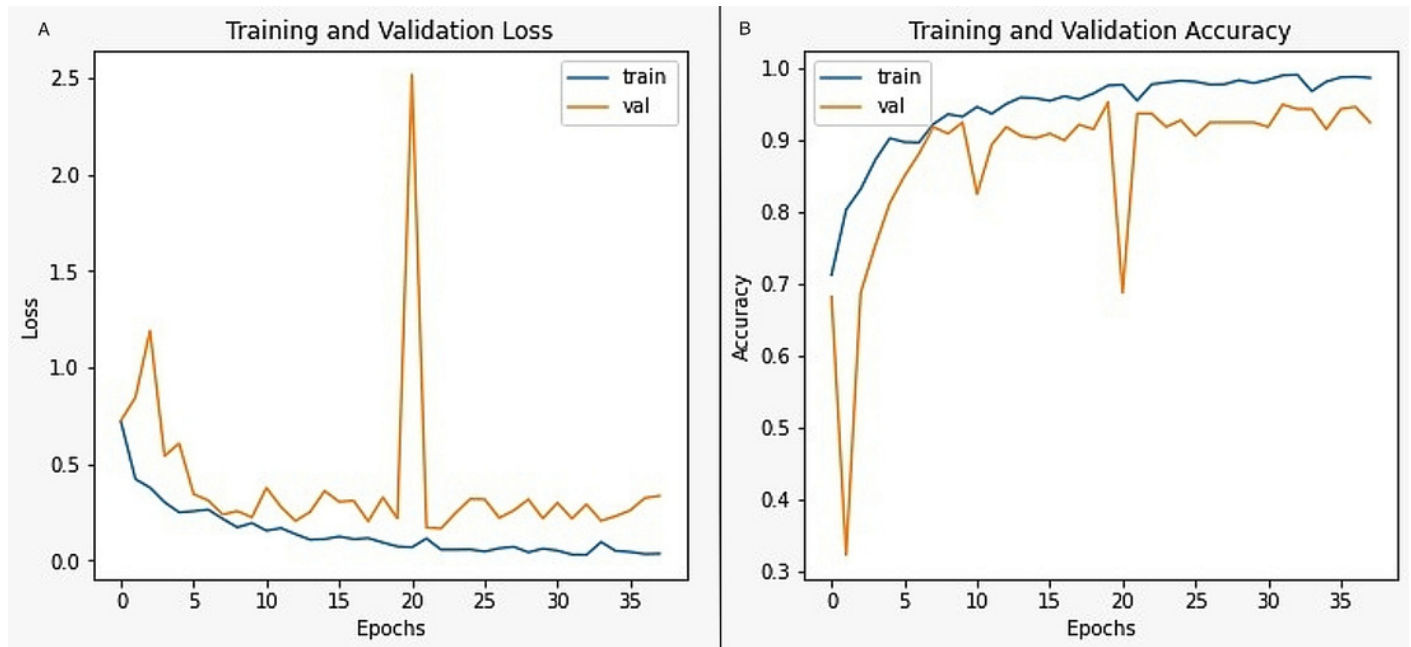
Figure 5

Output screens of proposed SLNS approach
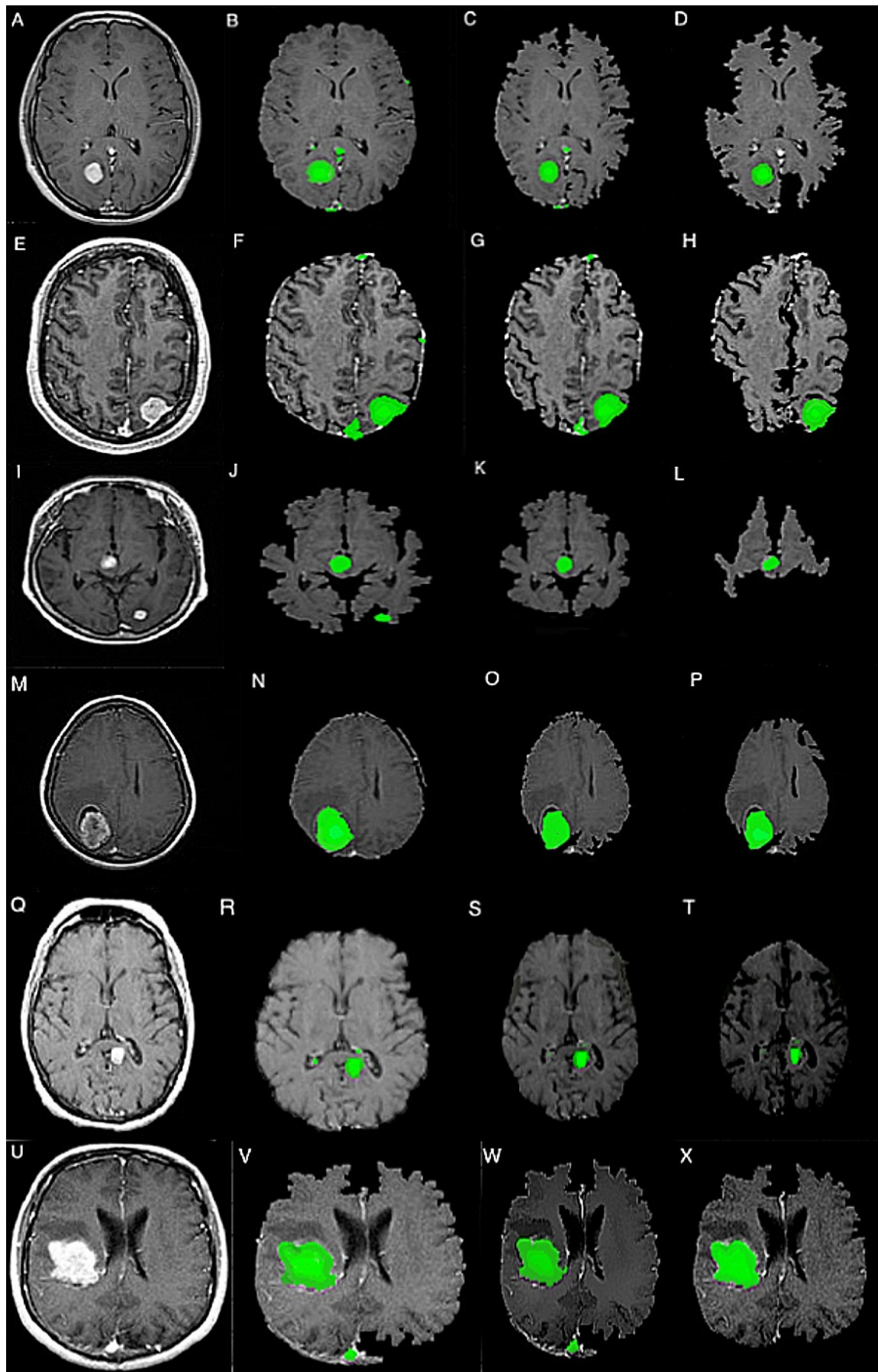
Figure 6

Graph representing the comparative analysis of various approaches
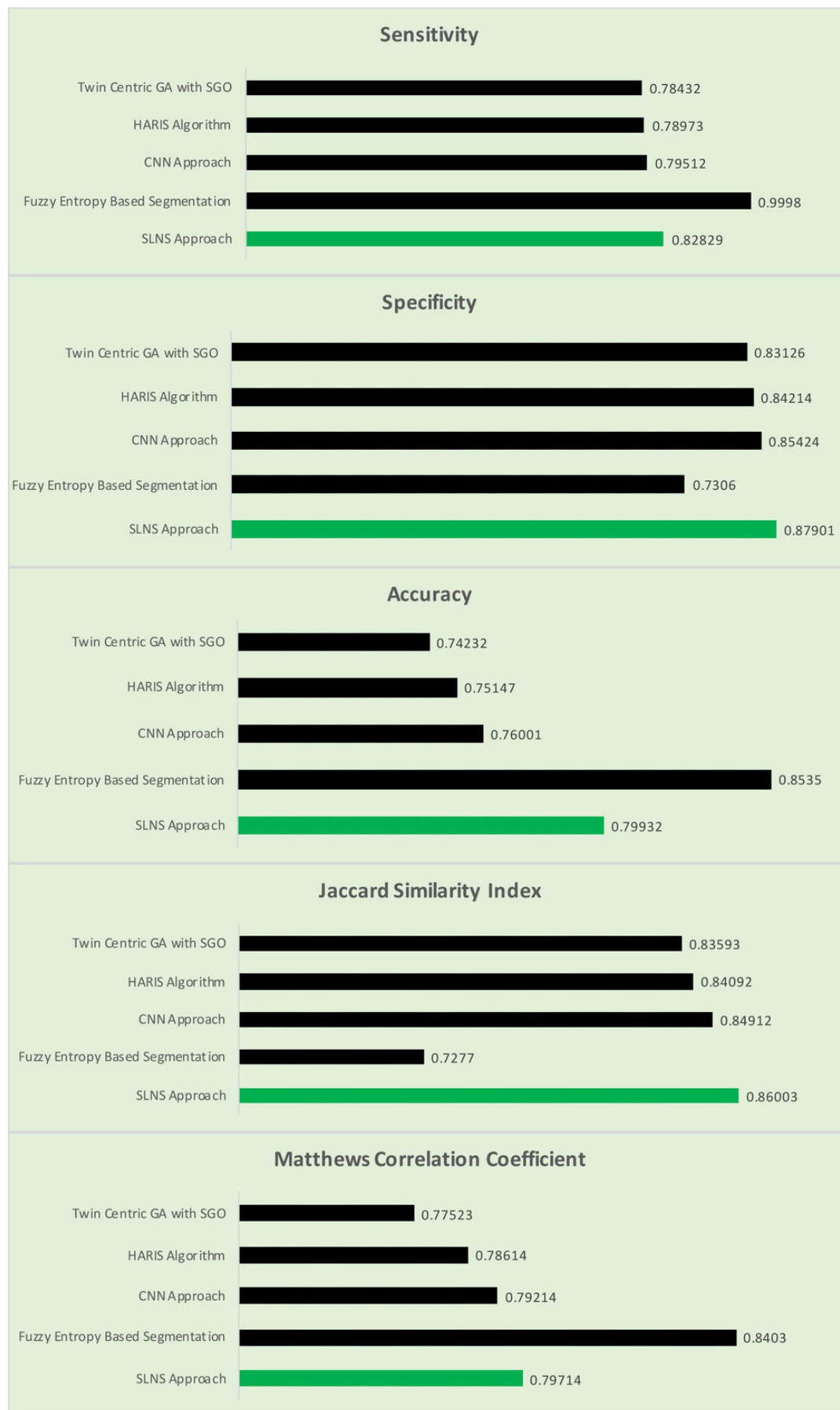
Figure 7

Graph representing the computational time of various approaches
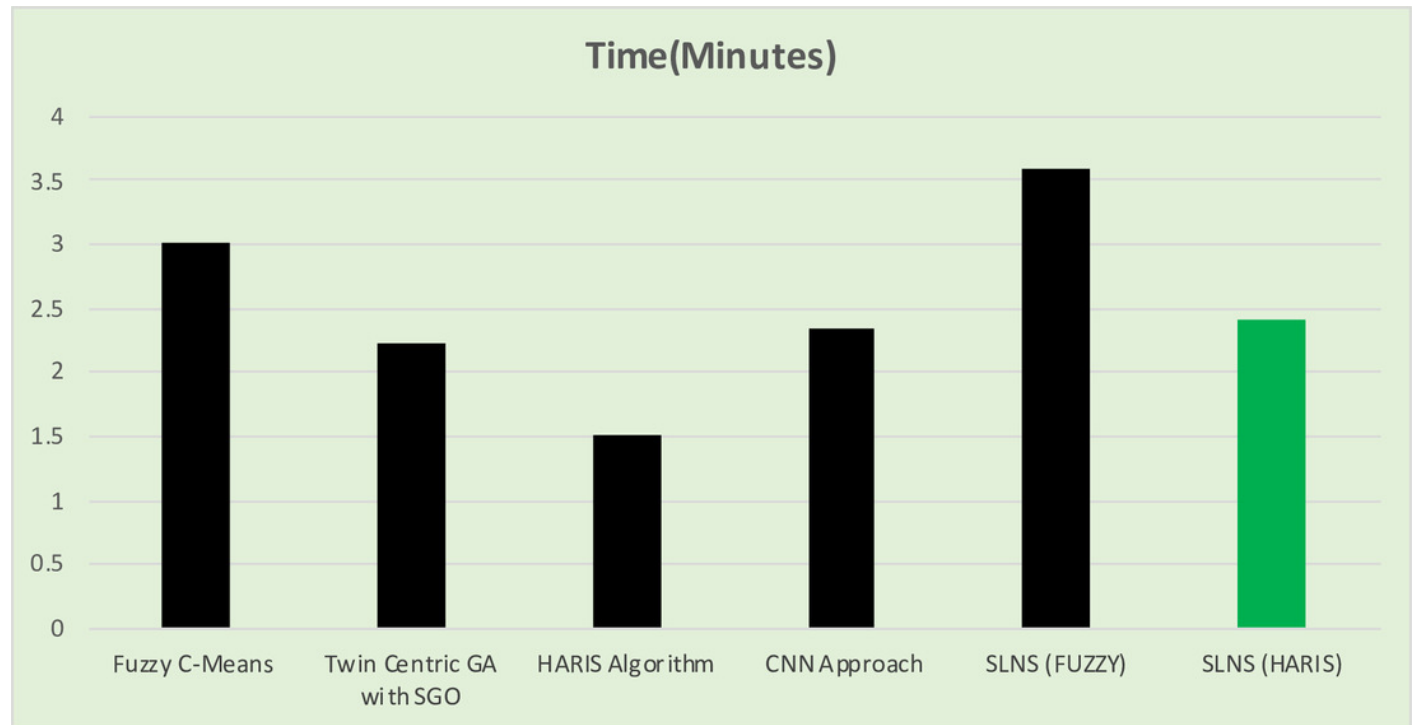
Table represents the confusion matrix of the proposed model

	SLNS through HARIS	SLNS through Fuzzy Membership
True Positive(%)	82.85	77.14
True Negative(%)	85.71	80.0
False Positive(%)	17.15	22.86
False Negative(%)	14.29	20.0

2
3

Table 1: Table represents the confusion matrix of the proposed model

Performance analysis of the proposed approach

	Sensitivity	Specificity	Accuracy	JSI	MCC
Twin Centric GA with SGO	0.78432	0.83126	0.74232	0.83593	0.77523
HARIS Algorithm	0.78973	0.84214	0.75147	0.84092	0.78614
CNN Approach	0.79512	0.85424	0.76001	0.84912	0.79214
Fuzzy Entropy Based Segmentation	0.99980	0.73060	0.85350	0.72770	0.84030
SLNS Approach	0.82829	0.87901	0.79932	0.86003	0.79714

2   Table 2: Table representing the performance analysis of the proposed approach

Table representing the performance analysis with Fuzzy Component

2

	Sensitivity	Specificity	Accuracy	JSI	MCC
SLNS with Fuzzy Membership	0.81218	0.86294	0.779383	0.8612	0.82490
SLNS with HARIS	0.80241	0.85815	0.76212	0.84899	0.79001

4   Table 3: Table representing the performance analysis with Fuzzy Component
5

Table representing the performance analysis of SLNS approach

	Tumor Core (TC)	Whole Tumor (WT)	Enhanced Tumor (ET)
Twin Centric GA with SGO	4.778±0.781	8.751±0.177	7.853±0.262
HARIS Algorithm	4.825±0.098	8.753±0.105	7.872±0.877
CNN Approach	4.823±0.245	8.756±0.714	7.870±0.011
SLNS with HARIS	4.824±0.781	8.754±0.911	7.874±0.982
SLNS with Fuzzy Membership	4.837±0.568	8.761±0.874	7.902±0.975

2   Table 4: Table representing the performance analysis of SLNS approach